New two- and three-dimensional non-oscillatory central finite volume methods on staggered Cartesian grids ☆

P. Arminjon [a,*], A. St-Cyr [b], A. Madrane [c]

[a] *Centre de Recherches Mathématiques, Université de Montréal, C.P. 6128, Succ. Centre-ville, Montréal, QC, Canada H3C 3J7*
[b] *Département de Mathématiques et de Statistiques, Université de Montréal, C.P. 6128, Succ. Centre-ville, Montréal, QC, Canada H3C 3J7*
[c] *German Aerospace Center, DLR Institute of Design Aerodynamics, Lilienthalplatz 7, 38108 Braunschweig, Germany*

Abstract

We present a 3D finite volume generalization of the 1-dimensional Lax–Friedrichs and Nessyahu–Tadmor schemes for hyperbolic equations on Cartesian grids. The non-oscillatory central difference scheme of Nessyahu and Tadmor, in which the resolution of the Riemann problem at the cell interfaces is by-passed thanks to the use of the staggered Lax–Friedrichs scheme, is extended here to a two-step, 3-dimensional non-oscillatory centered scheme in finite volume formulation.

Piecewise linear cell interpolants using several van Leer-type limiting techniques to estimate the gradient (van Leer, van Albada, SuperBee, MinMod) lead to a non-oscillatory spatial resolution of order superior to 1. The fact that the expected second-order resolution is not fully attained in 3D is investigated first by considering an alternate dual grid (in 2D), and by using the original van Albada limiter in 3D.

Numerical results for a linear advection problem with continuous and discontinuous initial conditions in 2D and 3D show the accuracy and stability of the method. A comparison is made between the 2D Arminjon–Stanescu–Viallon and Jiang–Tadmor formulations and the new one. A new simple projection method is used for the gradients in the new 2D scheme. We also include results for the 3D Euler system (channel with a forward facing step). © 2001 Published by Elsevier Science B.V. on behalf of IMACS.

0. Introduction

The non-oscillatory central difference scheme of Nessyahu and Tadmor may be interpreted as a Godunov-type scheme for one-dimensional hyperbolic conservation laws in which the resolution of the

Riemann problems at the cell interfaces is by-passed thanks to the use of the staggered Lax–Friedrichs scheme. Piecewise linear MUSCL-type cell interpolants and slope limiters lead to an oscillation-free second-order resolution.

In earlier papers [7–9] we presented a 2-dimensional finite volume method generalizing the one-dimensional Lax–Friedrichs [23] and Nessyahu–Tadmor [25] difference schemes for hyperbolic conservation laws to unstructured triangular grids, while in [2,5] we constructed a corresponding extension in the case of 2-dimensional Cartesian grids. These "central" finite volume methods share with the Lax–Friedrichs and Nessyahu–Tadmor schemes the two advantages of avoiding the resolution of Riemann problems at the cell interfaces, and being non-oscillatory.

In [18], Jiang and Tadmor have presented a slightly different extension to two-dimensional Cartesian grids; the difference between both extensions for rectangular grids is that in [5], the MUSCL (Monotonic Upstream-centered Scheme for Conservation Laws) variable extrapolation ("reconstruction technique") [32,33] is applied both to the vector of conservative variables and to the fluxes, while in [18], it is only used for the conservative variables. All these extensions to 2-dimensional problems lead to non-oscillatory, essentially second-order accurate finite volume methods.

In this paper, we first present a finite volume extension of the first-order accurate Lax–Friedrichs scheme to three-dimensional Cartesian grids, and show that the new scheme is monotone under an appropriate CFL condition. We then construct the corresponding extension of the Nessyahu–Tadmor difference scheme to a non-oscillatory finite volume method for 3-dimensional staggered Cartesian grids, which should in principle be second-order accurate.

As our first numerical experiments indicated orders between 0.8 and 1.3, we investigated two avenues to try and recover quasi-second-order accuracy. First in three dimensions, if we apply the simplified form of the van Albada limiter in the computation of the predictor, and any reasonable limiter for the gradient of the piecewise linear reconstruction at time t^n, we obtain accuracy orders between 0.7 and 1.86 depending on the choice of the limiter for the reconstruction step. Alternately, if we apply, as suggested by Venkatakrishnan [34], the *original* van Albada limiter [29], both to the reconstruction at time t^n and to the predictor at $t^{n+1/2}$, we obtain second-order resolution, in the L_1 norm, for an appropriate choice of the parameter K (see [34] and Section 1.7). Unfortunately, we then lose strict monotonicity preservation, and get small oscillations in computationally sensitive regions, e.g., near the supersonic inlet, as was the case in [34]. This is caused by the fact that the scheme leaves the reconstruction gradients unlimited or almost unlimited in the near-constant regions, as observed by Venkatakrishnan [30]. Choosing the smallest value of K compatible with second-order accuracy allows the limiter to remain active nearly everywhere except in regions where the solution is truly constant, and thus leads to nearly perfectly monotonous profiles where needed.

Our second field of investigation, as regards the recovery of second-order accuracy *and* preservation of monotonicity was related with our earlier construction [5], for 2-dimensional Cartesian grids, of a finite volume generalization of the Lax–Friedrichs (LF) and Nessyahu–Tadmor (NT) schemes. This generalization, for Cartesian grids, is not the direct transposition to rectangular grids of our earlier generalization of the LF and NT schemes to unstructured triangular grids [7,9]; indeed it features cells, both for the original and dual grid, with sides parallel to the x, y axes (Fig. 1(a)), while for the direct analogous to our triangular scheme, the alternate quadrilateral cells L_{lm} of the dual grid should in fact be *oblique*, with sides making 45 degree angles with the sides of the original cell C_{ij} (see Fig. 1(b) showing the dual cell L_{ij}).
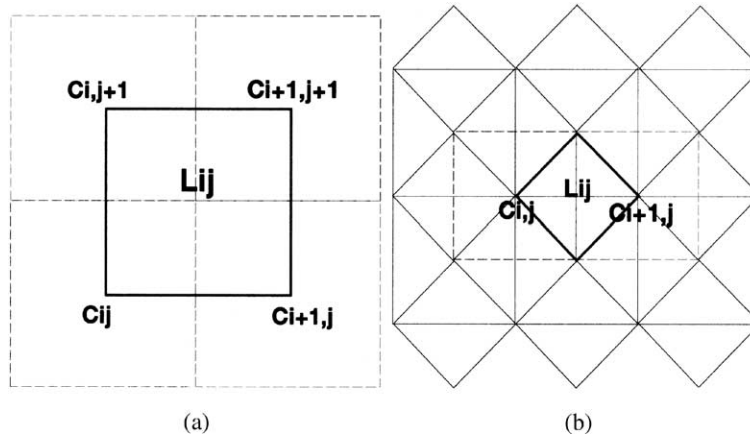
Fig. 1. 2D dual cells. (a) Original (non-oblique) case. (b) Oblique case.

This approach has been presented in [2,3], and has also been considered, independently, by Katsaounis and Levy [19]; one of the tests presented in [19] is the same as our first numerical test here, inspired from [18], and results are comparable since both schemes are very similar. With this new "oblique" version of our 2-dimensional finite volume extensions of the Lax–Friedrichs and Nessyahu–Tadmor schemes to staggered Cartesian grids, we obtain second-order accuracy and monotonicity preservation, provided that we use standard limiters, without having to apply the original or modified van Albada limiter.

In a forthcoming paper, we might extend this new "oblique dual grid" approach to the corresponding 3-dimensional finite volume method with oblique dual cells, and show that we again obtain, in the case of a linear advection problem with continuous initial function, second-order accuracy and monotonicity preservation without having to resort to special limiters such as the original van Albada limiter, and simply applying the 3-dimensional analog of the standard limiters successfully used with both 2-dimensional Cartesian versions (non-oblique dual rectangular cells [5], oblique dual cells as described in Section 2 of this paper) of the 2-dimensional finite volume method for Cartesian grids.

Regarding the actual accuracy one should expect to obtain, let us observe here that in the case of a nonlinear hyperbolic equation with a (discontinuous) initial function $u_0 \in L^\infty(\mathbb{R}^d) \cap BV_{\text{loc}}(\mathbb{R}^d)$, Küther [21,22] has recently proved an error estimate of order 0.25 for the Lax–Friedrichs-type finite volume scheme on unstructured grids, which is not optimal; it was indeed recently proved by Sabac [26] that $h^{1/2}$ is optimal for first-order schemes. For second-order schemes, it is presently believed/conjectured that h^1 is optimal. Küther's proof of the $h^{1/4}$-error estimate is inspired from the work of Haasdonk, Kröner and Rohle [14].

Instead of modifying the staggered/dual cells, another possible approach consisting of modifying the numerical flux by using an improved quadrature formula for the fluxes across the boundaries of the cells has recently been proposed by Lie and Noelle [24]. Their scheme is less sensitive to grid orientation effects and leads to an improved preservation of symmetries as compared with the original scheme considered here and in [2,5,18].

We have recently proposed a new version of our method for 1- and 2-dimensional Cartesian grids and 3-dimensional unstructured tetrahedral grids, where a new approach to compute the flux allows us to bypass the predictor step used in all of the above schemes, thus substantially reducing computing times [6].

The organization of this paper is as follows. In Section 1, we describe our 3-dimensional central finite volume methods of first- and second-order accuracy, which generalize the LF and NT schemes, respectively. The dual cells used here have sides parallel to the coordinate axes, as in [5]. The first-order accurate Lax–Friedrichs-type finite volume method is shown to be *monotone* under an appropriate CFL condition. We also describe the limiters used in this paper. In Section 2, we construct the direct analogue, for 2-dimensional Cartesian grids, of our finite volume generalization of the NT scheme for unstructured triangular grids. This 2-dimensional finite volume method has oblique dual cells. In Section 3, we present numerical experiments for the 3-dimensional method of Section 1 and for the 2-dimensional oblique dual cell method of Section 2, with, in the latter case, a comparison with our earlier 2-dimensional finite volume method with dual cell boundaries parallel to the axes, and with the Jiang–Tadmor variant of that method.

1. Three-dimensional finite volume extensions of the Lax–Friedrichs and Nessyahu–Tadmor schemes

In this section we briefly describe how to construct a 3D finite volume generalization of the Nessyahu–Tadmor (1D) scheme on Cartesian grids. A 2D extension (ASV [1]) on quadrilaterals, featuring non-oblique dual cells, was first proposed in 1995 by Arminjon et al. [5]. The ASV finite volume method differs from the Nessyahu–Tadmor scheme because not only the dependent variable vector U but also the fluxes are reconstructed using a MUSCL technique. Four items are needed to obtain the ASV formulation (on structured uniform hexahedrals), for each time step.

- A centered monotone scheme (which implies that this scheme is only first-order).
- A reconstruction of the solution with the MUSCL method to obtain second-order spatial accuracy.
- A predictor for the fluxes, for second-order time accuracy.
- A precise CFL condition to prevent wave interaction between the original and dual grids.

The first item is defined with the help of a staggered Lax–Friedrichs-type (LF) finite volume scheme. This scheme uses a uniform fully structured hexahedral grid for the dual grid. We also need to prove that this LF-type scheme is monotone. The reconstruction is then performed here both for the point values U_{ijk} and for the fluxes (see [5]). A predictor (in time) is then constructed by using a Taylor expansion combined with the conservation law (1). Finally, the CFL condition is computed using analytic and geometric arguments inspired by Hindmarsh et al. [9,15].

1.1. Generic model equation

We consider the 3-dimensional system of conservation laws

$$U_t + \nabla \cdot F(U) = U_t + f_x + g_y + h_z = 0, \tag{1}$$

where

$$U = (u^1, u^2, \ldots, u^m)^{\mathrm{T}},$$

$$F = (f, g, h) = ((f^1, f^2, \ldots, f^m)^{\mathrm{T}}, (g^1, g^2, \ldots, g^m)^{\mathrm{T}}, (h^1, h^2, \ldots, h^m)^{\mathrm{T}})$$

with the initial condition $U(x, y, z, 0) = U_0(x, y, z)$. System (1) will be assumed to be hyperbolic in the sense of the following definition.

---

[1] Arminjon–Stanescu–Viallon.

Definition 1.1. The system (1) is said to be hyperbolic if any linear combination of the $m \times m$ Jacobian matrices $A(U)$, $B(U)$, $C(U)$ where

$$\mathcal{A} = \big(A(U), B(U), C(U)\big) = \left(\frac{\partial f}{\partial U}, \frac{\partial g}{\partial U}, \frac{\partial h}{\partial U}\right) \tag{2}$$

has m real eigenvalues $\lambda^k(U)$ and m linearly independent right and left eigenvectors $r^k(U)$ and $l^k(U)$ that satisfy

$$r^i \cdot l^j = \delta_{ij}.$$

1.1.1. Notations

As the staggered Lax–Friedrichs and Nessyahu–Tadmor schemes are one-dimensional two-step schemes using two staggered grids at alternate time steps, our three-dimensional finite volume extensions also use two staggered grids and two time steps.

For the first grid, the control volume or cell is the region $C_{ijk} = [x_{i-1/2}, x_{i+1/2}] \times [y_{j-1/2}, y_{j+1/2}] \times [z_{k-1/2}, z_{k+1/2}]$, while for the second grid the dual cell will be defined as $L_{ijk} = [x_i, x_{i+1}] \times [y_j, y_{j+1}] \times [z_k, z_{k+1}]$.

1.2. First time step, LF-type scheme

In the first (and further odd) time step of our 3-dimensional finite volume schemes, we start from initial (or previously obtained) cell average values $U_{C_{ijk}}$ for the cells of the first grid, and compute cell average values $U_{L_{ijk}}$ for the (staggered) dual cells of the second grid. This is done by integrating (1) on an extended control volume $L_{ijk} \times [t^n, t^{n+1}]$, where L_{ijk} is a cell of the dual grid, and by assuming that $U_{L_{ijk}}(t^n + \Delta t)$ is piecewise constant on the cells of the second grid. The following equality is easily verified with the help of Fig. 2, showing dual cell L_{ijk} and one of its composing subcells $L_{ijk} \cap C_{lmn}$ in the particular case $l = i$, $m = j$, $n = k$ (dotted region).

$$L_{ijk} = \bigcup_{\substack{lmn \\ \text{neighbor}}} L_{ijk} \cap C_{lmn}, \tag{3}$$

where "lmn neighbor" means $l = i, i+1; m = j, j+1; n = k, k+1$ and in the sequel, $\sum_{lmn}()$ stands for $\sum_{lmn \text{ neighbor}}()$.

Using (1) and applying the divergence theorem to the flux term, we obtain

$$\int_{t^n}^{t^{n+1}} \int_{L_{ijk}} U_t \, dV \, dt + \int_{t^n}^{t^{n+1}} \int_{\partial L_{ijk}} F \cdot n \, dA \, dt = 0 \tag{4}$$

or

$$\int_{L_{ijk}} U(x, y, z, t^{n+1}) \, dV - \int_{L_{ijk}} U(x, y, z, t^n) \, dV = - \int_{t^n}^{t^{n+1}} \int_{\partial L_{ijk}} F(U(x, y, z, t)) \cdot n \, dA \, dt. \tag{5}$$

For a *first-order accurate Lax–Friedrichs-type method*, the right-hand side is evaluated (according to the left rectangular quadrature formula) at time t^n, using (3) and cell-average values:

$$V(L_{ijk})\boldsymbol{U}_{L_{ijk}}(t^{n+1}) - \sum_{lmn} V(C_{lmn} \cap L_{ijk})\boldsymbol{U}_{lmn}(t^n) = -\Delta t \int_{\partial L_{ijk}} \boldsymbol{F}(\boldsymbol{U}^n) \cdot \boldsymbol{n}\,\mathrm{d}A. \tag{6}$$

The function $V(\,)$ calculates the volume of the region common to the cell L_{ijk} (second grid) and cell C_{lmn} (first grid). Let us mention that the cells of either grid do not need to be cubic, in fact, they can be any rectangular prism in 3-space.

For a *second-order accurate method* generalizing the NT scheme, the right-hand side of (5) is evaluated with the midpoint formula for integration with respect to time

$$-\int_{t^n}^{t^{n+1}} \int_{\partial L_{ijk}} \boldsymbol{F}(\boldsymbol{U}(x,y,z,t)) \cdot \boldsymbol{n}\,\mathrm{d}A\,\mathrm{d}t \cong -\Delta t \int_{\partial L_{ijk}} \boldsymbol{F}(\boldsymbol{U}^{n+1/2}) \cdot \boldsymbol{n}\,\mathrm{d}A, \tag{7}$$

where $\boldsymbol{U}^{n+1/2}$ is some predicted value obtained with the help of (1). The corresponding calculations will be described in Section 1.6.

1.3. Second time step, LF-type scheme

Once the first time step is completed, starting from the obtained dual cell values $\boldsymbol{U}_{L_{ijk}}$, we compute cell average values $\boldsymbol{U}_{C_{ijk}}$ for the original cells C_{ijk} of the first grid; the calculations are performed in a similar manner (see [5,7,9] for details in the 2-dimensional case).

1.4. Fluxes

The computation of the flux for the scheme (right-hand side of (6)) is more complex than that of the conservative variables. Here, again, we assume that the fluxes are piecewise constant on ∂L_{ijk} and ∂C_{lmn}, respectively.

We begin by labeling each of the faces of ∂L_{ijk} and the corresponding normal vectors (Fig. 2):

$$\partial L_{ijk} = \partial L_{ijk}^1 \cup \partial L_{ijk}^2 \cup \partial L_{ijk}^3 \cup \partial L_{ijk}^4 \cup \partial L_{ijk}^5 \cup \partial L_{ijk}^6,$$

$$\boldsymbol{n}_1 = -\boldsymbol{n}_x, \qquad \boldsymbol{n}_2 = -\boldsymbol{n}_y, \qquad \boldsymbol{n}_3 = -\boldsymbol{n}_z, \tag{8}$$

$$\boldsymbol{n}_4 = \boldsymbol{n}_1, \qquad \boldsymbol{n}_5 = \boldsymbol{n}_2, \qquad \boldsymbol{n}_6 = \boldsymbol{n}_3, \tag{9}$$

$$\boldsymbol{n}_x = (1,0,0), \qquad \boldsymbol{n}_y = (0,1,0), \qquad \boldsymbol{n}_z = (0,0,1). \tag{10}$$

Again, one can derive an expression similar to (3) for the faces. Each one of the faces can be written as the union of 4 subfaces resulting from the intersection with the C_{lmn} of the first grid:

$$\partial L_{ijk}^q = \bigcup_{\substack{lmn \\ \text{neighbor}}} C_{lmn} \cap \partial L_{ijk}^q,$$

where the notation *neighbor* now means that only four of the eight index combinations corresponding to the notation $\bigcup_{lmn\ \text{neighbor}}$ give rise to a non-empty intersection set. If $A(\,)$ is a function that calculates the area of a given surface, the first step of the staggered LF scheme can be written in the following compact form:
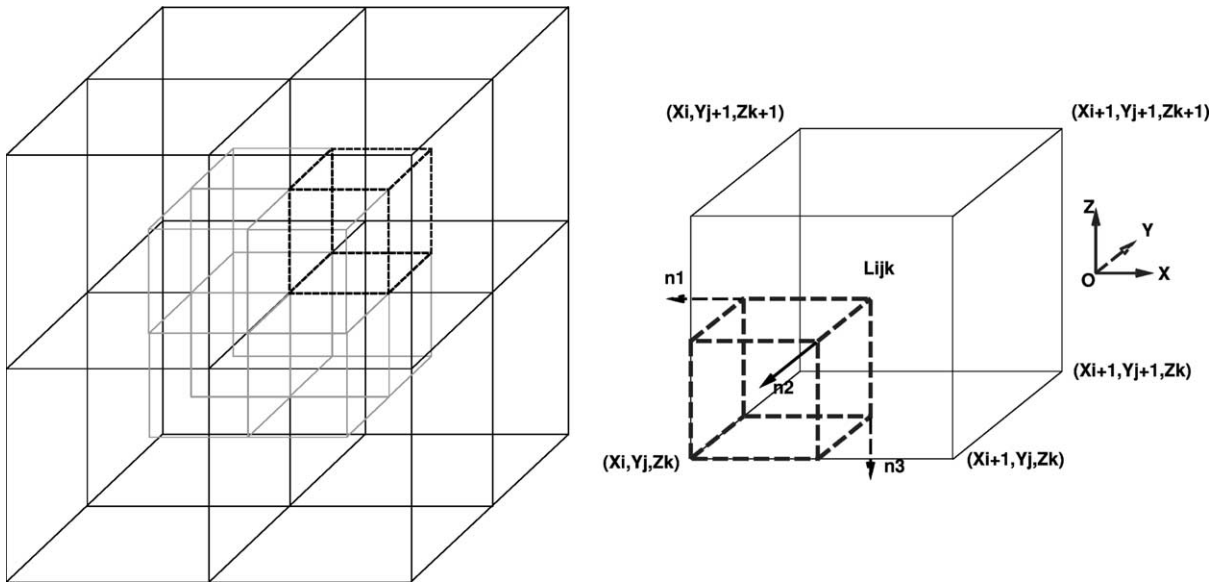
Fig. 2. Intersection of cell L_{ijk} and cell $C_{l=i,\,m=j,\,n=k}$ (dotted region).

$$\boldsymbol{U}_{L_{ijk}}\big(t^n + \Delta t\big) = \frac{1}{V(L_{ijk})}\left(\sum_{\substack{lmn \\ \text{neighbor}}} V(C_{lmn} \cap L_{ijk})\boldsymbol{U}_{lmn}\big(t^n\big) - \Delta t \sum_{q=1}^{6} \sum_{\substack{lmn \\ \text{neighbor}}} A\big(C_{lmn} \cap \partial L_{ijk}^q\big)\boldsymbol{F}_{lmn}\cdot\boldsymbol{n}_q \right),$$

(11)

where $\boldsymbol{F}_{lmn} = \boldsymbol{F}(\boldsymbol{U}_{lmn}(t^n))$ and $\boldsymbol{U}_{lmn}(t^n) = \boldsymbol{U}_{C_{lmn}}(t^n)$ for lmn neighbor.

1.5. Monotonicity condition

Let us recall here some basic definitions to make the article self-contained.

Definition 1.2. A general scheme for the model Eq. (1) can be written

$$\boldsymbol{U}_{L_{ijk}}^{n+1} = \mathcal{H}(\boldsymbol{U}_{C_{i-p,\,j-q,\,k-r}}, \ldots, \boldsymbol{U}_{C_{i+p',\,j+q',\,k+r'}}).$$

(12)

Our finite volume scheme is a subcase of the form

$$\boldsymbol{U}_{L_{ijk}}^{n+1} = \mathcal{H}(\boldsymbol{U}_{C_{i,j,k}}, \ldots, \boldsymbol{U}_{C_{i+1,\,j+1,\,k+1}}) = \mathcal{H}\big\{\boldsymbol{U}_{lmn}(t^n), (lmn \text{ neighbor})\big\}.$$

(13)

Definition 1.3. The scheme (13) is monotone if $\mathcal{H}$ is a monotone increasing function of each of its arguments

$$0 \leqslant \frac{\partial \mathcal{H}}{\partial \boldsymbol{U}_{lmn}} \quad (lmn \text{ neighbor})$$

or equivalently if all eigenvalues of the matrix $\partial \mathcal{H}/\partial \boldsymbol{U}_{lmn}$ (lmn neighbor) are non-negative.

Theorem 1.1. *Under the CFL-like condition* (22) *below, the 3-dimensional finite volume extension* (11) *of the LF scheme for structured uniform staggered grids is monotone.*

Proof. From (11) we find

$$\frac{\partial \mathcal{H}}{\partial \boldsymbol{U}_{lmn}} = \frac{V(C_{lmn} \cap L_{ijk})}{V(L_{ijk})} \mathcal{I} - \Delta t \sum_{q=1}^{6} \frac{A(C_{lmn} \cap \partial L_{ijk}^q)}{V(L_{ijk})} \mathcal{A}_{lmn} \cdot \boldsymbol{n}_q \tag{14}$$

for *lmn* neighbor. To simplify the calculations, we introduce the following vector:

$$\boldsymbol{K} = \sum_{q=1}^{6} \frac{A(C_{lmn} \cap \partial L_{ijk}^q)}{V(L_{ijk})} \boldsymbol{n}_q = (K_x, K_y, K_z). \tag{15}$$

We then have

$$\sum_{q=1}^{6} \frac{A(C_{lmn} \cap \partial L_{ijk}^q)}{V(L_{ijk})} \mathcal{A}_{lmn} \cdot \boldsymbol{n}_q = \mathcal{A}_{lmn} \cdot \sum_q \frac{A(C_{lmn} \cap \partial L_{ijk}^q)}{V(L_{ijk})} \boldsymbol{n}_q = \mathcal{A}_{lmn} \cdot \boldsymbol{K} \equiv \mathcal{M}. \tag{16}$$

Here, $\mathcal{M} = \mathcal{M}(l, m, n)$ represents a weighted sum of the 3 Jacobian matrices A, B, C. By our assumption on the hyperbolicity of system (1), the matrix $\mathcal{M}$ has real eigenvalues λ_s ($1 \leqslant s \leqslant m$) and can be diagonalized by a similarity transformation (see also [16, Vol. II, pp. 176–191] for the Euler equations). By Definition 1.3, monotonicity of our finite volume extension of the Lax–Friedrichs scheme will be established if we can prove, in view of (14)–(16), that

$$\mathcal{W} \equiv \frac{V(C_{lmn} \cap L_{ijk})}{V(L_{ijk})} \mathcal{I} - \Delta t \mathcal{M} \tag{17}$$

is positive semi-definite. By the spectral theorem, the eigenvalues of $\mathcal{W}$ are the numbers

$$\frac{V(C_{lmn} \cap L_{ijk})}{V(L_{ijk})} - \Delta t \lambda_s(\mathcal{M}), \tag{18}$$

where $\lambda_s(\mathcal{M})$ is an eigenvalue of $\mathcal{M}$. We therefore need

$$\Delta t \lambda_s(\mathcal{M}) \leqslant \frac{V(C_{lmn} \cap L_{ijk})}{V(L_{ijk})}, \quad s = 1, \dots, m, \ lmn \text{ neighbor}, \tag{19}$$

or, finally,

$$\Delta t \max_{1 \leqslant s \leqslant m} \{|\lambda_s(\mathcal{M})|\} \leqslant \frac{V(C_{lmn} \cap L_{ijk})}{V(L_{ijk})}. \qquad \square \tag{20}$$

Remark 1.1. It might appear at first sight that (20) does not have the dimensional form of a CFL condition; but the matrix $\mathcal{M}$ is equal to the matrix product $\mathcal{A}_{lmn} \cdot \boldsymbol{K}$ where $\boldsymbol{K}$ is obviously $O(h^{-1})$ by (15), where h is the mesh size in the x, y, z directions, for the case of a uniform rectangular grid. The eigenvalues $\lambda_s(\mathcal{M})$ are thus $O(h^{-1})$ and (20) does have the dimensions of a CFL condition.

Remark 1.2. For a perfectly uniform hexahedral grid the factor $V(C_{lmn} \cap L_{ijk})/V(L_{ijk})$ reduces to $\frac{1}{8}$, and the vector $\boldsymbol{K}$ takes the simpler form $\boldsymbol{K} = 1/(4h) \sum_{q=1}^{6} \delta(C_{lmn} \cap L_{ijk}) \boldsymbol{n}_q$, so that the monotonicity condition (20) is not very restrictive (here $\delta(\cdot)$ represents a "Kronecker-like" set function which is equal to zero when the argument is the empty set, otherwise its value is 1); indeed, we then obtain the condition

$$\frac{\Delta t}{h} \max_s \{|\lambda_s(\boldsymbol{U}_{lmn})|\} \leqslant \frac{1}{2}. \tag{21}$$

However this is only the monotonicity condition for a usual (non staggered) grid, the parameter h in (21) must be divided by two for obvious geometric reasons (since we are using staggered grids). The final monotonicity condition for the finite volume Lax–Friedrichs scheme can thus be written as

$$\frac{\Delta t}{h} \max_s \{ |\lambda_s(\boldsymbol{U}_{lmn})| \} \leqslant \frac{1}{4}. \tag{22}$$

Remark 1.3. In the scalar case, we can therefore expect the numerical solution u_h to converge to the unique solution of (1) satisfying the entropy condition, as $h \to 0$, if it does converge, see [10,12,20]. In the 2-dimensional case of unstructured triangular grids, we have proved [8], for a scalar linear hyperbolic equation, that the numerical solution satisfies a discrete maximum principle, and converges weakly* to a weak solution of (1). The proof can be directly extended to the case of 2-dimensional Cartesian grids, again for a scalar linear hyperbolic equation.

1.6. A second-order finite volume method via MUSCL cellwise interpolation

In the one-dimensional Nessyahu–Tadmor difference scheme, the first-order accuracy of the Lax–Friedrichs scheme was raised to second-order by the use of van Leer's MUSCL [32,33] cellwise piecewise linear interpolation of the conservative variables (but not of the flux functions), and a midpoint rule approach for the time discretization of the flux integral, implemented with a predictor–corrector treatment of each time step. In the 3-dimensional finite volume generalization, we apply the same strategy to both the conservative variables *and* the flux functions $\boldsymbol{f}, \boldsymbol{g}, \boldsymbol{h}$, following our 2-dimensional generalization of the NT scheme to Cartesian grids [5]. Let $M^U_{C_{lmn}}$ (respectively, $M^f_{C_{lmn}}$, $M^g_{C_{lmn}}$, $M^h_{C_{lmn}}$) denote the piecewise trilinear interpolant of the conservative variable $\boldsymbol{U}$ (respectively, of the flux functions $\boldsymbol{f}, \boldsymbol{g}, \boldsymbol{h}$) on cell C_{lmn}:

$$M^U_{C_{lmn}}(\boldsymbol{R}) = \boldsymbol{U}_{C_{lmn}} + \nabla \boldsymbol{U}_{C_{lmn}} \cdot (\boldsymbol{R} - \boldsymbol{R}_{C_{lmn}}), \tag{23}$$

where $\nabla \boldsymbol{U}_{C_{lmn}}$ is some limited approximate gradient of the interpolant, to be defined later (Section 1.7) (with similar definitions for $M^f_{C_{lmn}}$, etc.). $\boldsymbol{R}$ is the position vector of an arbitrary point contained in C_{lmn}, and $\boldsymbol{R}_{C_{lmn}}$ denotes the centroid of the same cell.

Replacing in (5) all the cellwise constant variables by their linear reconstruction (23), integrating in time with the help of the midpoint rule for the flux integral, we obtain

$$V(L_{ijk}) \boldsymbol{U}^{n+1}_{L_{ijk}} = \int_{L_{ijk}} M^U_{L_{ijk}} \, \mathrm{d}V - \Delta t \int_{\partial L_{ijk}} \left(M^{f^{n+1/2}}_{L_{ijk}} n_x + M^{g^{n+1/2}}_{L_{ijk}} n_y + M^{h^{n+1/2}}_{L_{ijk}} n_z \right) \mathrm{d}A, \tag{24}$$

where $M^U_{L_{ijk}}$ and $M^{f^{n+1/2}}_{L_{ijk}}$ are the piecewise linear interpolants of $\boldsymbol{U}$ and $\boldsymbol{f}^{n+1/2} = \boldsymbol{f}(\boldsymbol{U}(t^{n+1/2}))$, respectively, in cell L_{ijk}; $\boldsymbol{U}(t^{n+1/2})$ is a predicted value defined below.

We now use the definitions of the control volumes C_{ijk} and L_{ijk} and introduce the following notations:

$$\Delta x_i = x_{i+1/2} - x_{i-1/2}, \qquad \Delta y_j = y_{j+1/2} - y_{j-1/2}, \qquad \Delta z_k = z_{k+1/2} - z_{k-1/2},$$

$$V_{ijk} = \Delta x_i \Delta y_j \Delta z_k, \qquad A_{ij} = \Delta x_i \Delta y_j.$$

For a uniform and isotropic grid, $\Delta x_i = \Delta y_j = \Delta z_k \equiv h$.

For simplicity, from now on, U_{ijk} will mean $U_{C_{ijk}}$, i.e., the value of U at the centroid of the cell of the first grid. Decomposing the limited gradient into its Cartesian parts gives:

$$\nabla V_{ijk} = \left(V_{ijk,x}^{\lim}, V_{ijk,y}^{\lim}, V_{ijk,z}^{\lim} \right), \tag{25}$$

where for any vector function V, $V^{\lim}$ denotes the limited vector V. Our complete ASV-type (non-oblique Cartesian) 3D finite volume generalization of the NT scheme can now be derived and is given in Appendix A. The intermediate-time fluxes are found with the help of a predictor step:

$$U_{ijk}^{n+1/2} = U_{ijk}^n + \frac{\Delta t}{2} U_{ijk,t}(t^n). \tag{26}$$

Using the conservation equation (1), (26) can be written in a form which is easy to evaluate, replacing the gradients by their limited numerical approximations:

$$U_{ijk}^{n+1/2} = U_{ijk}^n - \frac{\Delta t}{2} \left(f_{ijk,x}^{\lim} + g_{ijk,y}^{\lim}, + h_{ijk,z}^{\lim} \right), \tag{27}$$

where $f_{ijk,x}^{\lim}$ denotes the limited derivative of f in the $\widehat{x}$ direction.

Here, an alternate choice for the predictor can be made, using the known Jacobian matrices of the flux function:

$$U_{ijk}^{n+1/2} = U_{ijk}^n - \frac{\Delta t}{2} \left(A \cdot U_{ijk,x}^{\lim, n} + B \cdot U_{ijk,y}^{\lim, n} + C \cdot U_{ijk,z}^{\lim, n} \right). \tag{28}$$

From a computational viewpoint, some inconveniences arise from the fact that (28) is very costly to evaluate even for the non-conservative Jacobians (which have a simpler form).

For each of these two predictors, two approaches to define the predicted values of the dependent variables at time t^{n+1} can be used. By a proper transformation (see [12,16]), one can pass from the conservative to the physical variables (when dealing with the Euler equations), make the prediction at $t^{n+1/2}$ and then use it to reconstruct the fluxes at $t^{n+1/2}$, to finally obtain U^{n+1}. The other approach is to use the predictor on the conservative variables, and then rebuild the fluxes with the intermediate-time approximations.

1.7. Limiters

To give a short description of the MUSCL cell interpolation considered here with the various limiters mentioned earlier in this section and used in our numerical experiments, we follow the notation used in [27,34], and consider *in the 1-dimensional case for simplicity* piecewise linear reconstructions defined, at the cell interface $x_{i+1/2}$, by

$$u_{i+1/2}^L = u_i + \tfrac{1}{2} \psi(\theta_i)(u_i - u_{i-1}), \tag{29}$$

$$u_{i-1/2}^R = u_i - \tfrac{1}{2} \psi\left(\frac{1}{\theta_i}\right)(u_{i+1} - u_i), \tag{30}$$

where

$$\theta_i = \frac{\Delta_+ u_i}{\Delta_- u_i} \equiv \frac{u_{i+1} - u_i}{u_i - u_{i-1}} \tag{31}$$

and $\psi(\theta)$ is the (slope) limiter function; we take $\psi(r) \equiv 0$ for $r \leqslant 0$. In this paper, we have used the following limiters.

(i) *Simplified van Albada* [2] (SVA). Let

$$\psi_{VA}(\theta) = \frac{\theta^2 + \theta}{\theta^2 + 1}. \tag{32}$$

With this limiter, (29) takes the form

$$u_{i+1/2}^L = u_i + \frac{1}{2} \frac{\theta^2 + \theta}{\theta^2 + 1} (u_i - u_{i-1}) \tag{33}$$

with $\theta_i = \Delta_+ u_i / \Delta_- u_i \equiv \Delta_+ / \Delta_-$, for simplicity.

We note here that if we use a cell interface value defined from a centered approximation of the slope

$$u_{i+1/2}^L = u_i + \frac{1}{2} R(\theta_i) \frac{u_{i+1} - u_{i-1}}{2} \tag{34}$$

van Albada's simplified limiter must now be written in the form

$$R(\theta_i) = \frac{2\theta_i}{1 + \theta_i^2}. \tag{35}$$

It can be easily verified that both (33) and (34) can be written as

$$u_{i+1/2}^L = u_i + \frac{1}{2} \frac{\Delta_+^2 \Delta_- + \Delta_-^2 \Delta_+}{\Delta_+^2 + \Delta_-^2}. \tag{36}$$

(ii) *Original van Albada* [3] (OVA). This choice corresponds to modifying Eq. (36) as follows:

$$u_{i+1/2}^L = u_i + \frac{1}{2} \frac{(\Delta_+^2 + \varepsilon^2)\Delta_- + (\Delta_-^2 + \varepsilon^2)\Delta_+}{\Delta_+^2 + \Delta_-^2 + 2\varepsilon^2}, \tag{37}$$

where ε^2 is made proportional to $(\Delta x)^3$, by setting $\varepsilon^2 = (K\Delta x)^3$ where K is a constant. Notice that at an extremum of u or in a region where u is nearly constant, $\varepsilon^2 = \mathrm{O}(h^3)$ will dominate Δ_+^2, Δ_-^2 by Taylor's theorem, leading to a nearly unlimited value $u_{i+1/2}^L$ (i.e., $\psi \approx 1$) in (29), while if K is very large the same situation will prevail. It has been verified by Venkatakrishnan that for a fixed value of K, the scheme will tend to be second-order accurate, but will not be monotonicity preserving for an advection problem. This difficulty arises from the fact that the scheme resumes to the unlimited form (34) with $R(\theta) = 1$ in the near-constant regions (see [34] for details). By restricting the action of the *original* van Albada limiter (37) to the neighborhood of true extrema only, while using the simplified form (32)–(36) elsewhere, Venkatakrishnan obtained a globally second-order accurate scheme (for all usual norms) which is monotonicity preserving (the limiter is then the original van Albada limiter at a true extremum, but the simplified van Albada in near-constant regions). In this paper, for simplicity, we chose the

---

[2] SVA: Simplified van Albada limiter. (We should mention here that in [34], the original and simplified van Albada limiters have been exchanged. Van Albada's original limiter really is defined by (37), as communicated to the first author by B. van Leer.)

[3] OVA: Original van Albada without Threshold.

following limiting strategy: Defining $u_i^{\max} = \max(u_{i-1}, u_i, u_{i+1})$ and reconstructions of the form $u_i(x) = u_i + \psi(\theta_i)(u_i - u_{i-1})/\Delta x(x - x_i)$ we use the original van Albada limiter (37) everywhere except when both $\widetilde{\Delta}_+ = n_i^{\max} - u_i$ and $\widetilde{\Delta} = u_i(x_{i+1/2}) - u_i$ are below a certain tolerance threshold, in which case we take the limiter equal to 1 (no limitation). This variant of the original van Albada limiter will be noted OVAT (Original van Albada with Threshold).

(iii) *van Leer* (VL). In van Leer's notation we consider piecewise linear interpolants

$$\widetilde{u}(x) = u_i + \delta_i \frac{(x - x_i)}{\Delta x}, \quad x_{i-1/2} \leqslant x \leqslant x_{i+1/2}, \tag{38}$$

with θ_i as in (31) and

$$\delta_i = R(\theta_i)\widehat{\delta}_i \quad \text{and} \quad \widehat{\delta}_i \equiv \frac{u_{i+1} - u_{i-1}}{2} \tag{39}$$

the coefficient $R(\theta_i)$ is a "slope limiter" related to Sweby's [28] flux limiter $\phi(r)$ by [12]

$$\phi_{VL}(r) = \frac{R(\theta)(1 + \theta)}{2\theta} \quad \text{with} \quad r_i = \frac{\Delta_- u_i}{\Delta_+ u_i} = \frac{1}{\theta_i}. \tag{40}$$

We then have [12,13] the corresponding forms of van Leer's limiters

$$R(\theta) = \frac{4\theta}{(1 + \theta)^2}, \quad \theta \geqslant 0, \tag{41}$$

and

$$\phi_{VL}(r) = \begin{cases} \dfrac{2r}{1 + r}, & r \geqslant 0, \\ 0, & r < 0. \end{cases} \tag{42}$$

(iv) *MinMod* (MM). In Sweby's notation, the minmod limiter is defined by

$$\phi_{MM}(r) = \begin{cases} \min(r, 1), & r \geqslant 0, \\ 0, & r < 0 \end{cases} \tag{43}$$

in the slope limiter notation

$$MM(\Delta_+, \Delta_-) = \tfrac{1}{2}\{\operatorname{sgn}(\Delta_+) + \operatorname{sgn}(\Delta_-)\} \min\{|\Delta_-|, |\Delta_+|\}. \tag{44}$$

(v) *SuperBee* (SB). In this case

$$\phi_{SB}(r) = \max\{0, \min(2r, 1), \min(r, 2)\}. \tag{45}$$

2. Two-dimensional Cartesian grid scheme with oblique dual cells ASCV[4]

Notations

We consider Eq. (1) with a flux function $\boldsymbol{F}(\boldsymbol{U}) = (\boldsymbol{f}(\boldsymbol{U}), \boldsymbol{g}(\boldsymbol{U}))$ in some rectangular region Ω of the x-y plane, with initial condition

$$\boldsymbol{U}(x, y, t = 0) = \boldsymbol{U}_0(x, y), \quad (x, y) \in \Omega. \tag{46}$$
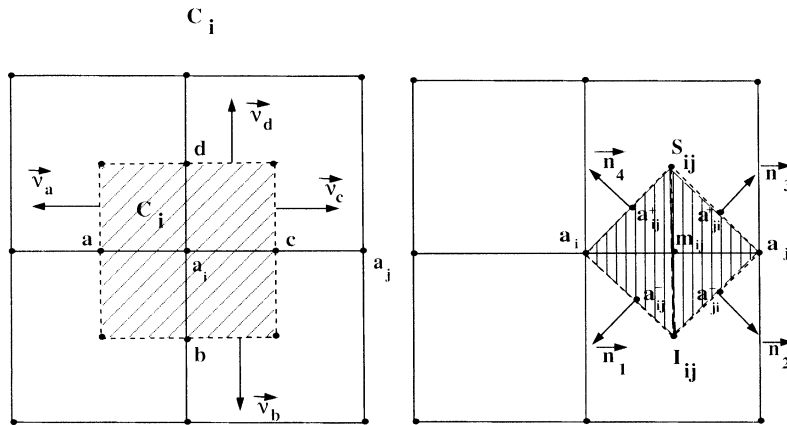
---

[4] Arminjon, St-Cyr, Viallon.

Fig. 3. Cell C_i and cell L_{ij}.

We shall describe the scheme in the case of a uniform rectangular grid which partitions Ω into M^2 squares of equal area; the extension to arbitrary rectangular grids is straightforward, except for the initialization, which requires numerical integration, and the programming part of the resolution, where we have to proceed as in the case of a fully unstructured grid. If $h = \Delta x = \Delta y = x_{i+1/2} - x_{i-1/2} = y_{j+1/2} - y_{j-1/2}$ is the mesh size, the nodes of the first grid are the points $(x_i, y_j) = (ih, jh)$ for $0 \leqslant i, j \leqslant M$. We introduce a numbering of these nodes, noted

$$a_i, \quad 1 \leqslant i \leqslant (M+1)(M+1), \tag{47}$$

and consider, for an arbitrary node a_i, the finite volume cell C_i defined, for the first grid, as the square (quadrilateral in the case of an arbitrary rectangular grid) obtained by joining the centroids of the four squares adjacent to a_i (Fig. 3). For the second (dual) grid, the nodes are the midpoints m_{ij} of sides such as a_i, a_j of the original grid. The corresponding oblique dual cell L_{ij} is defined by joining the points a_i, a_j to the centroids I_{ij} and S_{ij} of the squares sharing the common side $a_i a_j$.

Let $U_i^n \cong U(a_i, t^n)$ and $U_{ij}^{n+1} \cong U(m_{ij}, t^{n+1})$ denote the nodal or cell average values in the first and second grid at time t^n and t^{n+1}, respectively (n even). In the first step, we compute the approximation U_{ij}^{n+1} of the problem (1), (46) at the centroid of the oblique cell L_{ij}, using a finite volume approach.

First time step

Integrating (1) in the extended cell $L_{ij} \times [t^n, t^{n+1}] = [(L_{ij} \cap C_i) \cup (L_{ij} \cap C_j)] \times [t^n, t^{n+1}]$, we obtain

$$\int_{t^n}^{t^{n+1}} \iint_{L_{ij}} U_t \, dA \, dt = - \int_{t^n}^{t^{n+1}} \iint_{L_{ij}} \nabla \cdot F \, dA \, dt \tag{48}$$

or using Gauss' divergence theorem

$$\iint_{L_{ij}} U(x, y, t^{n+1}) \, dA = \iint_{L_{ij} \cap C_i} U(x, y, t^n) \, dA + \iint_{L_{ij} \cap C_j} U(x, y, t^n) \, dA - \int_{t^n}^{t^{n+1}} \int_{\partial L_{ij}} (f n_x + g n_y) \, d\sigma \, dt, \tag{49}$$

where the left-hand side defines the new cell value U_{ij}^{n+1}

$$A(L_{ij})U_{L_{ij}}^{n+1} \cong \iint\limits_{L_{ij}} U(x, y, t^{n+1}) \, dA. \tag{50}$$

The first two integrals in the right-hand side of (49) can be written as

$$\left(\iint\limits_{(L_{ij} \cap C_i)_S} + \iint\limits_{(L_{ij} \cap C_i)_I} \right) U(x, y, t^n) \, dA + \left(\iint\limits_{(L_{ij} \cap C_j)_S} + \iint\limits_{(L_{ij} \cap C_j)_I} \right) U(x, y, t^n) \, dA, \tag{51}$$

where

$$(L_{ij} \cap C_i)_S = \text{triangle } a_i m_{ij} S_{ij}, \qquad (L_{ij} \cap C_i)_I = \text{triangle } a_i I_{ij} m_{ij},$$

$$(L_{ij} \cap C_j)_S = \text{triangle } a_j S_{ij} m_{ij}, \qquad (L_{ij} \cap C_j)_I = \text{triangle } a_j m_{ij} I_{ij}.$$

Instead of splitting the integral on L_{ij} into the contributions of four triangles, as above, we can split it into only two triangles without changing the accuracy of the approximation. The decomposition into four triangles will be used for the right-hand side of (48).

For a uniform Cartesian grid we have, to second-order accuracy:

$$\iint\limits_{L_{ij}} U(x, y, t^n) \, dA \cong \left\{ U\left(x_i + \frac{\Delta x}{3}, y_i\right) A(L_{ij} \cap C_i) + U\left(x_j - \frac{\Delta x}{3}, y_j\right) A(L_{ij} \cap C_j) \right\}. \tag{52}$$

To obtain second-order accuracy and preserve monotonicity of the solution, we introduce van Leer's (MUSCL) piecewise linear interpolant, defined at a node a_i (in analogy with (23), (25)) by

$$\widetilde{U}_i(x, y, t^n) = U_i^n + U_{i,x}^{\lim, n} \frac{(x - x_i)}{\Delta x} + U_{i,y}^{\lim, n} \frac{(y - y_i)}{\Delta y}. \tag{53}$$

Combining (52) and (53) now gives

$$\int\limits_{L_{ij}} U(x, y, t^n) \, dA$$

$$\cong U_i^n A(L_{ij} \cap C_i) + U_j^n A(L_{ij} \cap C_j) + \tfrac{1}{3} U_{i,x}^{\lim, n} A(L_{ij} \cap C_i) - \tfrac{1}{3} U_{j,x}^{\lim, n} A(L_{ij} \cap C_j). \tag{54}$$

In the flux integral, the integration with respect to time can be approximated, to second-order accuracy, by the midpoint rule; the right-hand side of (48) is thus approximated by

$$\Delta t \int\limits_{\partial L_{ij}} \left(f(U(x, y, t^{n+1/2}))n_x + g(U(x, y, t^{n+1/2}))n_y \right) d\sigma \tag{55}$$

which requires a prediction at the intermediate time $t^{n+1/2}$, both for U and for the fluxes, at the cell interfaces; for example, we need a prediction at the midpoint a_{ij}^- of line segment $a_i I_{ij}$ (Fig. 3) to comply with the AV formulation [7–9]; this had not been applied in [5], where we had used a MUSCL reconstruction of the fluxes combined with an evaluation, at time $t^{n+1/2}$, performed directly at the vertices. We feel it is the extension of this procedure which is, in 3 dimensions, responsible (at least in part) for the loss of accuracy mentioned in the introduction, even though all steps of the approximations are in fact time-and-space second-order accurate.

We will use the following prediction at a_{ij}^-, considered as the value along line segment $a_i I_{ij}$:

$$U_{a_i I_{ij}}^{n+1/2} = \widetilde{U}_i(a_{ij}^-, t^n) + \frac{\Delta t}{2} U_t(a_{ij}^-, t^n). \tag{56}$$

In view of (1), we get

$$U_{a_i I_{ij}}^{n+1/2} = \widetilde{U}_i(a_{ij}^-, t^n) - \frac{\Delta t}{2}\left(A(\widetilde{U}_i(a_{ij}^-, t^n))U_{i,x}^{\lim} + B(\widetilde{U}_i(a_{ij}^-, t^n))U_{i,y}^{\lim}\right). \tag{57}$$

We note $f(U_{a_i I_{ij}}^{n+1/2})$ the corresponding predicted flux computed at the midpoint a_{ij}^- of $a_i I_{ij}$, at time $t^{n+1/2}$, with the help of (57). For a uniform square grid, the quadrilateral cell L_{ij} is in fact a square rotated by 45 degrees. The unit vectors normal to the boundary of L_{ij} (Fig. 3) are

$$\boldsymbol{n}_1 = -\frac{\sqrt{2}}{2}(1, 1), \qquad \boldsymbol{n}_2 = \frac{\sqrt{2}}{2}(1, -1), \qquad \boldsymbol{n}_3 = \frac{\sqrt{2}}{2}(1, 1), \qquad \boldsymbol{n}_4 = \frac{\sqrt{2}}{2}(-1, 1). \tag{58}$$

By (55), the right-hand side of (48) is thus approximated as follows:

$$\int_{t^n}^{t^{n+1}} \int_{\partial L_{ij}} (f\boldsymbol{n}_x + g\boldsymbol{n}_y)\, d\sigma\, dt$$

$$= \int_{t^n}^{t^{n+1}} \left(\sum_{q=1}^4 \int_{\partial L_{ij}^q} (f\boldsymbol{n}_{x,q} + g\boldsymbol{n}_{y,q})\, d\sigma\right) dt$$

$$= \Delta t \frac{\sqrt{2}}{2}\Big((-f(U_{a_i I_{ij}}^{n+1/2}) - g(U_{a_i I_{ij}}^{n+1/2}))l(a_i I_{ij}) + (f(U_{a_j I_{ij}}^{n+1/2}) - g(U_{a_j I_{ij}}^{n+1/2}))l(a_j I_{ij})$$

$$+ (f(U_{a_j S_{ij}}^{n+1/2}) + g(U_{a_j S_{ij}}^{n+1/2}))l(a_j S_{ij}) + (-f(U_{a_i S_{ij}}^{n+1/2}) + g(U_{a_i S_{ij}}^{n+1/2}))l(a_i S_{ij})\Big).$$

For the rotated square cell L_{ij}, we have

$$l(a_i I_{ij}) = l(\partial_{ij}^1) = \frac{\sqrt{2}}{2}h.$$

The first time step then takes the following form:

$$U_{L_{ij}}^{n+1} A(L_{ij}) = \frac{h^2}{4}\big((U_i^n + U_j^n) + \tfrac{1}{3}(U_{i,x}^{\lim} - U_{j,x}^{\lim})\big)$$

$$- \tfrac{1}{2}h\Delta t\Big((-f(U_{a_i I_{ij}}^{n+1/2}) - g(U_{a_i I_{ij}}^{n+1/2})) + (f(U_{a_j I_{ij}}^{n+1/2}) - g(U_{a_j I_{ij}}^{n+1/2}))$$

$$+ (f(U_{a_j S_{ij}}^{n+1/2}) + g(U_{a_j S_{ij}}^{n+1/2})) + (-f(U_{a_i S_{ij}}^{n+1/2}) + g(U_{a_i S_{ij}}^{n+1/2}))\Big) \tag{59}$$

hence

$$U_{L_{ij}}^{n+1} = \tfrac{1}{2}(U_i^n + U_j^n) + \tfrac{1}{6}(U_{i,x}^{\lim} - U_{j,x}^{\lim})$$

$$- \frac{\Delta t}{h}\Big((-f(U_{a_i I_{ij}}^{n+1/2}) - g(U_{a_i I_{ij}}^{n+1/2})) + (f(U_{a_j I_{ij}}^{n+1/2}) - g(U_{a_j I_{ij}}^{n+1/2}))$$

$$+ (f(U_{a_j S_{ij}}^{n+1/2}) + g(U_{a_j S_{ij}}^{n+1/2})) + (-f(U_{a_i S_{ij}}^{n+1/2}) + g(U_{a_i S_{ij}}^{n+1/2}))\Big). \tag{60}$$

For a dual grid cell L_{ik} such that $a_i a_k$ is parallel to the y axis, some minor changes are necessary and we obtain

$$
\begin{aligned}
U_{L_{ik}}^{n+1} = {} & \tfrac{1}{2}(U_i^n + U_k^n) + \tfrac{1}{6}(U_{i,x}^{\lim} - U_{k,x}^{\lim}) \\
& - \frac{\Delta t}{h}\Big(\big(f(U_{a_k I_{ij}}^{n+1/2}) + g(U_{a_k I_{ij}}^{n+1/2})\big) + \big(-f(U_{a_k I_{ij}}^{n+1/2}) + g(U_{a_k I_{ij}}^{n+1/2})\big) \\
& \quad + \big(-f(U_{a_i S_{ij}}^{n+1/2}) - g(U_{a_i S_{ij}}^{n+1/2})\big) + \big(-f(U_{a_i S_{ij}}^{n+1/2}) - g(U_{a_i S_{ij}}^{n+1/2})\big)\Big).
\end{aligned}
\tag{61}
$$

2.1. Second time step

For the second (and further even) time step, we consider the original cell C_i (Fig. 3) and the time interval $t^{n+1} \to t^{n+2}$ (n even). Proceeding as for the first step, we obtain

$$
\begin{aligned}
U_{C_i}^{n+2} A(C_i) &= \iint\limits_{C_i} U(x, y, t^{n+2})\, dA \\
&\cong \iint\limits_{C_i} U(x, y, t^{n+1})\, dA - \Delta t \int\limits_{\partial C_i} \big(f(x, y, t^{n+3/2}) v_x + g(x, y, t^{n+3/2}) v_y\big)\, d\sigma.
\end{aligned}
\tag{62}
$$

The first integral in the right-hand side can be decomposed into 8 parts, and obvious symmetries in the case of a uniform square grid reduce this to 4 parts:

$$
\begin{aligned}
\iint\limits_{C_i} U(x, y, t^{n+1})\, dA = {} & \frac{h^2}{4}\Bigg(\Big(U_c^{n+1} - \frac{1}{6}U_{c,x}^{\lim,\,n+1}\Big) + \Big(U_d^{n+1} - \frac{1}{6}U_{d,y}^{\lim,\,n+1}\Big) \\
& + \Big(U_a^{n+1} + \frac{1}{6}U_{a,x}^{\lim,\,n+1}\Big) + \Big(U_b^{n+1} + \frac{1}{6}U_{b,y}^{\lim,\,n+1}\Big)\Bigg).
\end{aligned}
\tag{63}
$$

The flux integral is treated as above, using the unit normal vectors

$$
v_a = (-1, 0), \qquad v_b = (0, -1), \qquad v_c = (1, 0), \qquad v_d = (0, 1)
$$

we obtain

$$
\begin{aligned}
\int\limits_{\partial C_i} (f v_x + g v_y)\, d\sigma \cong {} & \frac{\Delta t}{2}\Big(f(U_{c_{-1/2}}^{n+3/2}) + f(U_{c_{1/2}}^{n+3/2}) - f(U_{a_{1/2}}^{n+3/2}) - f(U_{a_{-1/2}}^{n+3/2}) \\
& + g(U_{d_{1/2}}^{n+3/2}) + g(U_{d_{-1/2}}^{n+3/2}) - g(U_{b_{-1/2}}^{n+3/2}) + g(U_{b_{1/2}}^{n+3/2})\Big).
\end{aligned}
$$

The second step of the scheme can therefore be written as

$$
\begin{aligned}
U_{C_i}^{n+2} A(C_i) = {} & \frac{h^2}{4}\big(U_a^{n+1} + U_b^{n+1} + U_c^{n+1} + U_d^{n+1}\big) \\
& + \frac{h^2}{24}\big(U_{b,y}^{\lim,\,n+1} - U_{d,y}^{\lim,\,n+1} + U_{a,x}^{\lim,\,n+1} - U_{c,x}^{\lim,\,n+1}\big) \\
& - \frac{\Delta t\, h}{2}\Big(f(U_{c_{-1/2}}^{n+3/2}) + f(U_{c_{1/2}}^{n+3/2}) - f(U_{a_{1/2}}^{n+3/2}) - f(U_{a_{-1/2}}^{n+3/2}) \\
& \qquad + g(U_{d_{1/2}}^{n+3/2}) + g(U_{d_{-1/2}}^{n+3/2}) - g(U_{b_{-1/2}}^{n+3/2}) + g(U_{b_{1/2}}^{n+3/2})\Big).
\end{aligned}
\tag{64}
$$

3. Numerical experiments

Numerical experiments for the methods presented in Sections 1 and 2 will be described in the next two subsections.

3.1. Three-dimensional ASV formulation (non-oblique dual cells)

3.1.1. Linear advection

We consider the scalar advection equation

$$u_t + au_x + bu_y + cu_z = 0$$

with initial condition $u(x, y, z, 0) = u_0(x, y, z) \equiv f_0^{\text{test}}$ where (a, b, c) will be chosen equal to $(1, 1, 1)$ here. We consider the cases of a discontinuous and of a continuous initial function:

$$f_0^{\text{test 1}}(x, y, z) = \begin{cases} 0.5 & \text{if } (x, y, z) \in \left[\frac{7}{20}, \frac{12}{20}\right]^3, \\ 0 & \text{else}, \end{cases}$$

$$f_0^{\text{test 2}}(x, y, z) = \cos(2\pi x)\cos(2\pi y)\cos(2\pi z).$$

The spatial computational domain for both tests is the cube $[0, 1] \times [0, 1] \times [0, 1]$. In Table 1, L^1 denotes the error calculated with the L^1 norm, and N is the number of intervals in each spatial direction. In Tables 1 and 2, SVA/VL means that the simplified van Albada limiter was used for the prediction and the van Leer limiter for the reconstruction, with similar signification for SVA/MM, SVA/SB (i.e., predictor/reconstruction).

Table 1 shows the results for the discontinuous initial function; we note that in three dimensions, the limiters which are smoother give better accuracy, as has generally been observed in the literature [17,34].

Table 1
L^1-error and accuracy order, discontinuous problem (test 1) 3D case

Limiters	$L^1, N = 16$	$L^1, N = 32$	$L^1, N = 64$	O_{L^1}
OVAT[a] ($K = 3$)	0.010696	0.006992	0.003764	0.75
VL[b]	0.006030	0.004317	0.002083	0.77
MM[c]	0.014622	0.011124	0.007142	0.52
SB[d]	0.014158	0.010627	0.006385	0.57
SVA[e]/VL	0.009184	0.007319	0.003732	0.65
SVA/MM	0.011052	0.011415	0.007090	0.21
SVA/SB	0.010967	0.011116	0.006692	0.36

[a] Original van Albada with Threshold.
[b] Van Leer.
[c] MinMod.
[d] Superbee.
[e] Simplified van Albada.

Table 2
L^1 error and accuracy order, continuous problem (test 2), 3D case

Limiter	$L^1, N = 16$	$L^1, N = 32$	$L^1, N = 64$	O_{L^1}
SVA	0.032720	0.009580	0.002794	1.77
SVA/VL	0.023744	0.006406	0.001813	1.86
SVA/MM	0.047324	0.011864	0.003920	1.80
SVA/SB	0.021896	0.009090	0.002803	1.48

Table 3
Continuous problem (test 2) original van Albada limiter, 3D case

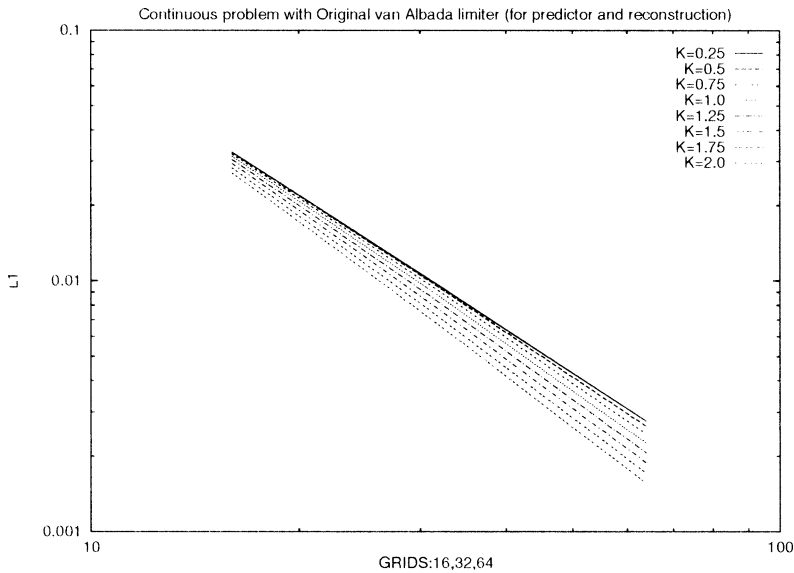| N	L^1 ($K = 0$)	O_{L^1}	L^1 ($K = 0.75$)	O_{L^1}	L^1 ($K = 1.5$)	O_{L^1}
8	0.095168		0.032114		0.029454	
16	0.032720	1.54	0.009070	1.82	0.007669	1.94
32	0.009580	1.77	0.002444	1.89	0.001876	2.03

Fig. 4. L^1 error Original van Albada limiter with $K \in [0.25, 2.25]$.

These results give some insight into the difficulties encountered in 3-dimensional calculations. We observe that the second grid refinement is much more efficient than the first; the order O_{L^1} indicated in the last column is the average of the two orders obtained from each grid refinement.

Tables 2 and 3 present a test with a continuous initial function. We see that with the smoother simplified van Albada and van Leer limiters, second-order accuracy is approached while it is even slightly exceeded with the original van Albada limiter.

Fig. 4 shows the effect of varying the parameter K in $\varepsilon^2 = (K \Delta x)^3$. For small values of K (say less than 3) the order increases with K, but we found that monotonicity is no longer preserved if K grows beyond a particular value which depends on the smoothness of the initial function; smoother data allow higher values of K before encountering monotonicity breaches.

3.1.2. Three-dimensional Euler equations

We considered the classical test problem [35] of supersonic flow in a channel with a forward facing step, extended here to a three-dimensional geometry corresponding to the computational domain $[0, 3] \times [0, 1] \times [0, 1]$ (in dimensionless units). The length, width and height of the step are 2.4, 1 and 0.2, respectively.
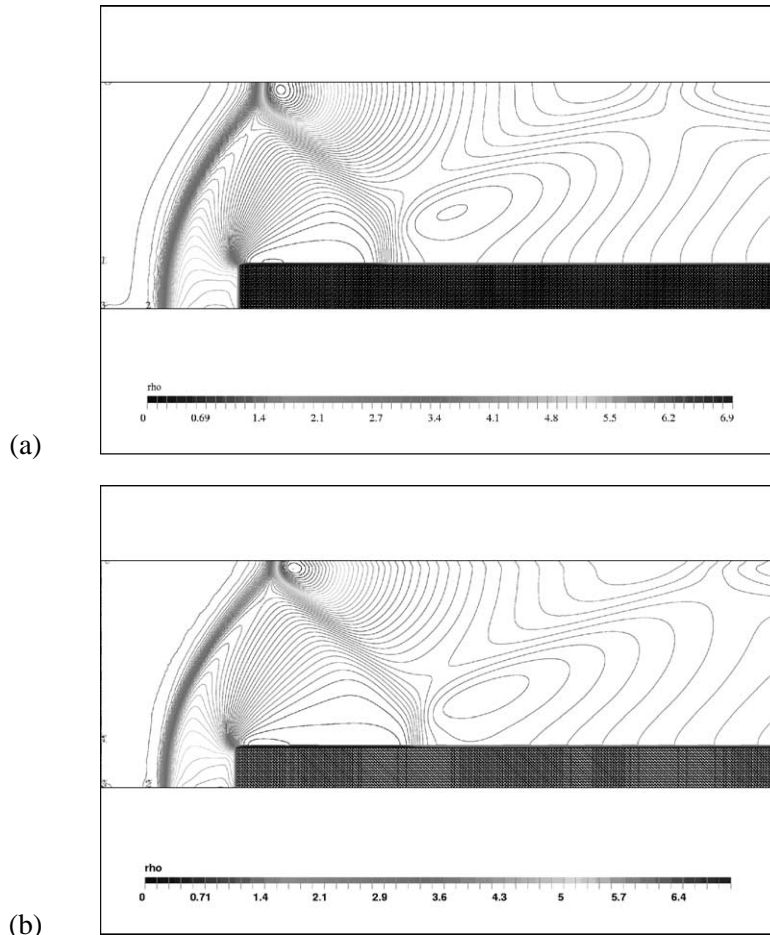

(a)

(b)

Fig. 5. Density $t = 3.05$, 61 contours, grid $240 \times 10 \times 80$; (a) Simplified van Albada and (b) OVAT[5] with $K = 3$.

Fig. 5(a) shows the results obtained (in the unstationary mode) with the simplified van Albada limiter, at time $t = 3.05$. Although the density contours are smooth, the forward shock is not very sharp and the reflected ones even weaker.

Fig. 5(b) presents the results obtained with the original van Albada limiter, with $K = 3$. The forward and reflected shocks are somewhat sharper, but we are still far from the sharp structure observed, e.g., in [5,35]. This is not only the consequence of some difficulties which might have been encountered by our method, but can also be attributed, at least in part, to the fact that we are dealing with three-dimensional shocks. Our results here compare favorably, though, with similar results presented, for the second-order upwind scheme and unstructured tetrahedra obtained from an original structured cubic grid, where the cubes are decomposed into tetrahedra, in [11]. We believe that mesh adaptation, which, unfortunately, was not available when our numerical experiments were performed, would lead to significant improvements, in the 3-dimensional case, as was observed in [1] in the 2D case, and intend to study this aspect of our 3D computations in the future.

3.2. New 2D ASCV formulation (oblique dual cells)

We considered initial values problems for the advection equation

$$u_t + au_x + bu_y = 0, \quad 0 \leqslant x, y \leqslant 1,$$

where we chose $a = b = 1$ here, with the initial functions

$$f_0^{\text{test 1}}(x, y) = \begin{cases} 0.5 & \text{if } \left(x - \frac{1}{2}\right)^2 + \left(y - \frac{1}{2}\right)^2 < \frac{1}{8}, \\ 0 & \text{elsewhere}, \end{cases}$$

and

$$f_0^{\text{test 2}}(x, y) = \sin(\pi(x + y)).$$

Table 4 shows the results obtained, for the discontinuous initial function, with the new "oblique dual cell" ASCV finite volume method, using the simplified van Albada limiter (SVA). N is the number of intervals in each spatial direction, and N_t is the number of double time steps. On the right, for comparison's sake, we have given the results obtained with the former ASV method (with cell boundaries parallel to the x or y axes), using van Leer's limiter (VL).

For this discontinuous problem, both methods seem to be comparable. The slight advantage provided by the ASV method could be due to the reconstruction of the fluxes and the fact that van Leer's limiter might, in some cases, lead to better results than the simplified van Albada limiter, as already observed for our 3-dimensional tests (Tables 1 and 2).

Table 4
Test 1, new 2D scheme ASCV (*left*) old scheme ASV (*right*)

N	N_t	SVA		van Leer	
Errors:		L^1	L^∞	L^1	L^∞
85	30	1.149E−2	2.615E−1	5.835E−3	2.929E−1

---

[5] OVAT: Original van Albada with Threshold.

Table 5
Test 2, new 2D scheme ASCV

	ASCV			
N	L^1	L^∞	O_{L^1}	O_{L^∞}
40	2.352E−2	6.003E−2		
80	5.759E−3	2.303E−2	2.03	1.38
160	1.347E−3	8.759E−3	2.10	1.39

Table 6
Test 2, 2D NT

	Jiang–Tadmor [18]			
N	L^1	L^∞	O_{L^1}	O_{L^∞}
40	1.93E−2	4.91E−2		
80	5.70E−3	2.12E−2	1.76	1.21
160	1.55E−3	8.90E−3	1.88	1.25

For the second (continuous) test function, we have compared the new oblique dual cell method (Table 5) with the results obtained by Jiang and Tadmor [18] for the same test (Table 6) with a 2-dimensional extension of the Nessyahu–Tadmor scheme similar to the ASV extension but without reconstruction of the fluxes.

The new ASCV method leads to better L^1 and L^∞ errors with the final grid, and to higher orders of accuracy. We note that we have performed 400 double time steps, while the number of time steps performed in [18] is not indicated.

4. Concluding remarks

We have presented new 2- and 3-dimensional non-oscillatory central finite volume methods for staggered grids. Starting from our two-dimensional finite volume generalization for Cartesian grids of the Nessyahu–Tadmor 1-dimensional finite difference scheme, we have extended it to a 3-dimensional finite volume method using two staggered Cartesian grids at alternate time steps. Our numerical experiments have shown that for continuous initial data, the method is non-oscillatory and second-order accurate when coupled with the original van Albada limiter; slight under/overshoots, for discontinuous data, can arise for inadequate choices of the limiter parameter K. Mesh adaptation would probably bring substantial improvements, and will be studied.

Having observed these under/overshoots when using the original van Albada limiter, and orders of accuracy inferior to the theoretical second-order predicted, in the absence of discontinuities, by the principle of the method when using the simplified van Albada limiter, and in an effort to simplify the computational complexity of our earlier 2-dimensional method, where the reconstruction step was

applied both to the dependent variables and to the fluxes, we have investigated here the possibility of a direct transposition of our 2-dimensional finite volume method for staggered unstructured triangular grids to the case of 2-dimensional Cartesian grids. This new "oblique dual cell" (or "diamond" dual cell) method (ASCV) seems to converge faster in all norms than the Jiang–Tadmor 2-dimensional extension of the NT scheme, while having comparable accuracy; on the other hand, its accuracy is comparable with the earlier 2-dimensional version (ASV) (non-oblique dual cells), but computing times are reduced since we do not reconstruct the fluxes; the 2-dimensional ASCV method can therefore be considered as a slight improvement of both earlier methods (ASV and JT).

These considerations have encouraged us to proceed to three-dimensional computations on unstructured tetrahedral grids, using grid adaptation [4].

Acknowledgements

Appendix A

Using Eq. (11) and the reconstruction (23), the complete ASV second-order scheme in 3D can be written as:

First time step.
(i) Reconstruction of conservative variables:

$$M_{C_{lmn}}^{U^n}(\boldsymbol{R}_{ijk}) = \boldsymbol{U}_{C_{lmn}}^n + \tfrac{1}{2}\nabla \boldsymbol{U}_{C_{lmn}}^n \cdot (\boldsymbol{R}_{ijk} - \boldsymbol{R}_{C_{lmn}}). \tag{A.1}$$

$\boldsymbol{R}_{ijk}$ represents the center of cell L_{ijk} and $\boldsymbol{R}_{C_{lmn}}$ the center of cell C_{lmn}.

(ii) Predictor:

$$\boldsymbol{U}_{ijk}^{n+1/2} = \boldsymbol{U}_{ijk}^n - \frac{\Delta t}{2}\big(A \cdot \boldsymbol{U}_{ijk,x}^{\lim,\,n} + B \cdot \boldsymbol{U}_{ijk,y}^{\lim,\,n} + C \cdot \boldsymbol{U}_{ijk,z}^{\lim,\,n}\big). \tag{A.2}$$

(iii) Reconstruction of the flux:

$$\boldsymbol{F}_{ijk}^{n+1/2} = \boldsymbol{F}\big(\boldsymbol{U}_{ijk}^{n+1/2}\big), \qquad M_{C_{lmn}}^{F^{n+1/2}}(\boldsymbol{R}_{\partial L_{ijk}^q}) = \boldsymbol{F}_{C_{lmn}}^{n+1/2} + \nabla \boldsymbol{F}_{C_{lmn}}^{n+1/2} \cdot (\boldsymbol{R}_{\partial L_{ijk}^q} - \boldsymbol{R}_{C_{lmn}}), \quad \text{(A.3)}$$

$\boldsymbol{R}_{\partial L_{ijk}^q}$ is the center of face q of the L_{ijk} cell.

Using the facts that $\Delta x = \Delta y = \Delta z = h$ and $V(C_{lmn} \cap L_{ijk})/V(L_{ijk}) = \tfrac{1}{8}$ and $A(C_{lmn} \cap \partial L_{ijk}^q)/V(L_{ijk}) = 1/(4h)$, Eq. (11) can be re-written as

(iv) Corrector:

$$\boldsymbol{U}_{L_{ijk}}^{n+1} = \frac{1}{8} \sum_{\substack{lmn \\ \text{neighbor}}} M_{C_{lmn}}^{\boldsymbol{U}^n}(\boldsymbol{R}_{ijk}) - \frac{\Delta t}{4h} \sum_{q=1}^{6} \sum_{\substack{lmn \\ \text{neighbor}}} M_{C_{lmn}}^{\boldsymbol{F}^{n+1/2}}(\boldsymbol{R}_{\partial L_{ijk}^q}) \cdot \boldsymbol{n}_q. \tag{A.4}$$

Second time step.

Repeat steps (i)–(iv) starting from the values on the staggered grid L_{ijk}.

References

[1] P. Arminjon, A. Madrane, Staggered mixed finite volume/finite element method for the Navier–Stokes equations, AIAA J. 37 (1999) 1558–1571.

[2] P. Arminjon, A. Madrane, A. St-Cyr, New Lax–Friedrichs-type finite volume schemes on 2 and 3D Cartesian staggered grids, in: J. Militzer (Ed.), 7th Annual Conference of the CFD Society of Canada, Halifax, Nova Scotia, 1999, pp. (3-3)–(3-10).

[3] P. Arminjon, A. Madrane, A. St-Cyr, New 2 and 3-dimensional non-oscillatory central finite volume methods on staggered Cartesian grids, Research Report CRM-2675, Centre de Recherches Mathématiques, Univ. de Montréal, 2000.

[4] P. Arminjon, A. Madrane, A. St-Cyr, Numerical simulation of 3-D flows with a non-oscillatory central scheme on staggered unstructured tetrahedral grids, in: H. Freistühler, G. Warnecke (Eds.), Proc. 8th Internat. Conf. on Hyperbolic Problems, Magdeburg, Germany, 2000.

[5] P. Arminjon, D. Stanescu, M.C. Viallon, A two-dimensional finite volume extension of the Lax–Friedrichs and Nessyahu–Tadmor schemes for compressible flows, in: M. Hafez, K. Oshima (Eds.), Proc. of the 6th Internat. Symp. on Computational Fluid Dynamics, Vol. 4, Lake Tahoe, NV, 1995, pp. 7–14.

[6] P. Arminjon, A. St-Cyr, New Lax–Friedrichs-type finite volume schemes in 1, 2 and 3D without time predictor step, in: G.E. Schneider (Ed.), Proc. of the 9th Annual Conference of the CFD Society of Canada, Kitchener, Ontario, 2001, pp. 63–68.

[7] P. Arminjon, M.C. Viallon, Généralisation du schéma de Nessyahu–Tadmor pour une équation hyperbolique à deux dimensions d'espace, C. R. Acad. Sci. Paris Ser. I 320 (1995) 85–88.

[8] P. Arminjon, M.C. Viallon, Convergence of a finite volume extension of the Nessyahu–Tadmor scheme on unstructured grids for a two-dimensional linear hyperbolic equation, SIAM J. Numer. Anal. 36 (3) (1999) 738–771.

[9] P. Arminjon, M.C. Viallon, A. Madrane, A finite volume extension of the Lax–Friedrichs and Nessyahu–Tadmor schemes for conservation laws on unstructured grids, Internat. J. Comput. Fluid Dynamics 9 (1) (1997) 1–22; Restricted version, 1994.

[10] M. Crandall, A. Majda, Monotone difference approximations for scalar conservation laws, Math. Comp. 34 (149) (1980) 1–21.

[11] M. Geiben-Wierse, Higher order upwind schemes for the compressible Euler equations in time-dependent geometries in 3D, Dissertation Thesis, Universität Freiburg, Germany, 1994.

[12] E. Godlewski, P.A. Raviart, Numerical Approximation of Hyperbolic Systems of Conservation Laws, Springer, New York, 1996.

[13] E. Godlewski, P.A. Raviart, Hyperbolic Systems of Conservations Laws, Editions Ellipses, Paris, 1991.

[14] B. Haasdonk, D. Kröner, C. Rohde, Convergence of a staggered Lax–Friedrichs Scheme for nonlinear conservation laws on unstructured two-dimensional grids, Preprint No. 07/2000, Mathematische Fakultät, University of Freiburg, Germany, April 2000; also Numer. Math. 88 (2001) 459–484.

[15] A.C. Hindmarsh, P.M. Gresho, D.F. Griffiths, The stability of explicit Euler time integration for certain finite difference approximations of the multidimensional advection diffusion equation, Internat. J. Numer. Methods Fluids 4 (1984) 853–897.

[16] C. Hirsch, Numerical Computation of Internal and External Flows, Vol. I, Wiley, New York, 1988; Vol. II, Wiley, New York, 1990.

[17] A. Jameson, Essential elements of computational algorithms for aerodynamic analysis and design, ICASE Report No. 97-68, 1997.

[18] G. Jiang, E. Tadmor, Non-oscillatory central schemes for multidimensional hyperbolic conservation laws, SIAM J. Sci. Comput. 19 (6) (1998) 1892–1917.

[19] T. Katsaounis, D. Levy, A modified structured central scheme for 2D hyperbolic conservation laws, Appl. Math. Lett. 12 (6) (1999) 86–89.

[20] S.N. Kruzhkov, First-order quasilinear equations with several space variables, Mat. Sb. 123 (1970) 228–255; English translation: Math. USSR-Sb. 10 (1970) 217–243.

[21] M. Küther, A priori and a posteriori error estimates for the staggered Lax–Friedrichs scheme in multi-dimensions for scalar nonlinear conservation laws, Preprint No. 19/2000, Mathematische Fakultät, University of Freiburg, Germany, 2000.

[22] M. Küther, Error estimates for the staggered Lax–Friedrichs Scheme on unstructured grids, SIAM J. Numer. Anal. 39 (4) (2001) 1269–1301.

[23] P.D. Lax, Weak solutions of nonlinear hyperbolic equation and their numerical computation, Comm. Pure Appl. Math. 7 (1954) 159–193.

[24] K.-A. Lie, S. Noelle, Remarks on high-resolution non-oscillatory central schemes for multidimensional systems of conservation laws. Part I: An improved quadrature rule for the flux computation, Preprint No. 679, Sonderforschungsbereich 256, Rheinische Friedrich-Wilhelms-Universität, Bonn, Germany, 2000.

[25] H. Nessyahu, E. Tadmor, Non-oscillatory central differencing for hyperbolic conservation laws, J. Comput. Phys. 87 (2) (1990) 408–463.

[26] F. Sabac, The optimal convergence rate of monotone finite difference methods for hyperbolic conservation laws, SIAM J. Numer. Anal. 34 (6) (1997) 2306–2318.

[27] S.P. Spekreijse, Multigrid solution of monotone second-order discretizations of hyperbolic conservation laws, Math. Comp. 49 (1987) 135–156.

[28] P.K. Sweby, High resolution schemes using flux limiters for hyperbolic conservation laws, SIAM J. Numer. Anal. 21 (1984) 995–1011.

[29] G.D. van Albada, B. van Leer, W.W. Roberts, A comparative study of computational methods in cosmic gas dynamics, Astron. Astrophys. 108 (1982) 76–84.

[30] B. van Leer, Towards the ultimate conservative difference scheme II. Monotonicity and conservation combined in a second order scheme, J. Comput. Phys. 14 (1974) 361–370.

[31] B. van Leer, Towards the ultimate conservative difference scheme III. Upstream-centered finite difference schemes for ideal compressible flow, J. Comput. Phys. 23 (1977) 263–275.

[32] B. van Leer, Towards the ultimate conservative difference scheme IV. A new approach to numerical convection, J. Comput. Phys. 23 (1977) 276–299.

[33] B. van Leer, Towards the ultimate conservative difference scheme V. A second-order sequel to Godunov's method, J. Comput. Phys. 32 (1979) 101–136.

[34] V. Venkatakrishnan, Convergence to steady state solutions of the Euler equations on unstructured grids with limiters, J. Comput. Phys. 118 (1995) 120–130.

[35] P. Woodward, P. Colella, The numerical simulation of two-dimensional fluid flow with strong shocks, J. Comput. Phys. 54 (1984) 115–173.